Observability of Flow-Dependent Structure Functions for Use in Data Assimilation

CRISTINA LUPU AND PIERRE GAUTHIER

Department of Earth and Atmospheric Sciences, Université du Québec à Montréal, Montréal, Québec, Canada

(Manuscript received 18 March 2010, in final form 19 October 2010)

ABSTRACT

One of the objectives of data assimilation is to produce initial conditions that will improve the quality of forecasts. Studies on singular vectors and sensitivity studies have shown that small changes to the initial conditions can sometimes lead to exponential error growth. This has motivated research to include flow-dependent structures within the assimilation that would have the characteristics to correctly predict the growth or decay of meteorological systems. This relates to the characterization of precursors to atmospheric instability. In this paper, the observability of such structures by observations is discussed. Several studies have shown that deploying observations over regions where changes in the initial conditions may impact the forecast the most do not lead to the expected benefit. In this paper, it is shown that given the small magnitude of the signal to be detected, it is important to take into account the accuracy of the observations. If the signal-to-noise ratio is too low, observations cannot detect and characterize precursors to forecast error growth. From that perspective, the assimilation only has the possibility to extract information about evolved structures of error growth. Experiments with a simple one-dimensional variational data assimilation (1D-Var) system are presented and, then, an adapted three-dimensional variational data assimilation (3D-Var) system with different sensitivity structure functions is used. The results have been obtained by adapting the variational assimilation system of Environment Canada.

1. Introduction

The accuracy of analyses produced by data assimilation systems depends on the precision of background and observation error covariances specified as input. The modeling and estimation of these covariances is critical for any data assimilation system in the context of numerical weather prediction (NWP). Algorithms like the three-dimensional variational data assimilation (3D-Var) produce analyses by blending together observations near the analysis time with a background state provided by a short-term numerical weather prediction. In this case, the background-error statistics are taken to be stationary and do not reflect the flow dependency of error growth that depends on the particular meteorological situation. Flow-dependent covariances can be obtained from approximate forms of the Kalman filter like the ensemble Kalman filter (Evensen 1994; Houtekamer et al. 2009).

Instabilities in atmospheric flows can be triggered by small perturbations to initial conditions and these can be characterized using adjoint methods that enable us to trace back the source of errors in a forecast to errors in the analysis. Lacarra and Talagrand (1988) showed that it is possible to characterize the structure of perturbations to the initial conditions that would lead to the most significant growth over a finite period of time. Those correspond to the so-called *singular vectors* that define the unstable subspace containing those perturbations that will experience the most significant error growth. This has been the foundation of the design of ensemble prediction systems that aim to determine how errors in the analysis and the model will lead to forecast errors in the medium range (Molteni et al. 1996; Buizza et al. 2007a).

Since it is possible to characterize those regions where perturbations in the analysis can lead to important error growth, the next logical step was to use this information to deploy observations in those areas where a reduction in the analysis error could lead to the most important reduction of the forecast error. This is the basis of targeting methods, which use information from singular vector or sensitivity gradients to plan the deployment of

Corresponding author address: Cristina Lupu, European Centre for Medium-Range Weather Forecasts, Shinfield Park, Reading, RG2 9AX, United Kingdom.
E-mail: cristina.lupu@ecmwf.int

DOI: 10.1175/2010MWR3424.1

adaptive observations. The Fronts and Atlantic Storm Track Experiment (FASTEX) campaign (Joly et al. 1999) was the first to test targeting methods and observations were deployed according to *sensitivity gradients*. Other campaigns followed like the North Pacific Experiment (NORPEX; Langland et al. 1999), the 2003 Atlantic The Observing System Research and Predictability Experiment (THORPEX) Regional Campaign (ATReC; Petersen and Thorpe 2007; Langland 2005a) and recently, the 2008 THORPEX Pacific-Asia Regional Campaign (T-PARC). From all those campaigns, the conclusions are that the impact of observations deployed over *sensitive areas* in the extratropics identified from singular vectors is, on average, about twice that of any other single observation, but the overall impact is small because of the large volume of data now assimilated (Langland 2005b; Kelly et al. 2007; Buizza et al. 2007b; Cardinali et al. 2007). These results bring us to reconsider the value of expensive observation campaigns for the sole purpose of assessing if targeted observations do lead to significant reduction of the forecast error. The current wisdom is that, if observations are to be deployed, it is then appropriate to take into account sensitivity information to do it. Particularly, this may be valuable for adaptive data selection for satellite data. Currently, because of limitations in the assimilation systems, a small fraction of the incoming volume of satellite data can be assimilated (Liu and Rabier 2002). Adaptive data selection is now being considered to assess whether this results in improvements in the quality of forecasts.

Fisher and Andersson (2001) have proposed a reduced-rank Kalman filter (RRKF) that restricts the evolution of the background-error covariances within an unstable subspace spanned by singular vectors. Their experimentation was thorough and went all the way to include the RRKF to provide the background-error covariances for the European Centre for Medium-Range Weather Forecasts (ECMWF) four-dimensional variational data assimilation (4D-Var). This was found to lead to a positive but small impact on the resulting forecasts, which was not deemed significant enough to implement this approach in the ECMWF operational suite. Currently, hybrid approaches have been proposed in which ensemble methods are used to define a subspace that is appropriate to describe the evolved background-error covariances (Buehner et al. 2010a,b; Berre et al. 2009). The preliminary results are very positive and this has sparked a renewed interest to include flow-dependent background-error covariances when cycling a 4D-Var assimilation system.

This paper's objective is to investigate some issues associated with the use of sensitivity information in the representation of background-error covariances with a 3D-Var assimilation system. Hello and Bouttier (2001) did propose an approach through which a priori sensitivity information from a single singular vector was included within the background-error covariance matrix, denoted by $\mathbf{B}$. Their approach is called an adapted 3D-Var as it includes some flow dependency. The a priori sensitivity was used to deploy targeted data during the FASTEX campaign (Hello et al. 2000). In the present paper, a variant of their algorithm is presented and tested both in a simple one-dimensional variational data assimilation (1D-Var) context and in 3D-Var. The rationale on which this study is based is the following.

The 24- or 48-h forecast error can be evaluated by comparing it with respect to a verifying analysis, and the adjoint of the forecast model can be used to define the change in initial conditions that would reduce the forecast error. This is referred to as *key analysis errors*, a term coined by Klinker et al. (1998) and has been the object of several studies afterward (Laroche et al. 2002; Langland et al. 2002; Caron et al. 2007a). This will be referred to as an a posteriori sensitivity function because it can only be obtained as a diagnostic of the origin of forecast error. In addition, a priori structure functions defined either as leading singular vectors (SVs) or from the gradient sensitivity vector method (Hello et al. 2000) are tools that have been widely applied in sensitivity studies, particularly for the development of targeting techniques. In the gradient sensitivity vector method, the cost function can be defined with respect to a particular aspect of the forecast at a later time and then to find out what are the changes to the initial conditions that will have the greatest impact on the forecast error growth. For example, taking the average of surface pressure of a 24-h forecast over an area of interest, one can then identify areas where changes in the current analysis could have a significant impact as defined by the sensitivity cost function. In Hello et al. (2000), this has been used to identify those regions where small changes to the initial conditions can be expected to lead to substantial changes in the forecast.

If a posteriori key analyses, as proposed by Klinker et al. (1998), do result in a dramatic reduction of forecast error, it would make sense to use those as structure functions within the $\mathbf{B}$ matrix so that observations would be used to define its amplitude. What was expected is that the amplitude of the key analysis would be recovered. However, this is not what happened. On second thought, the signal that was to be recovered was very small, which raised the question whether those structures could be detected at all by the observations, which contain some amount of observation error.

The paper is organized as follows. Section 2 briefly presents the formulation of the variational 3D-Var data assimilation system and its *adapted* 3D-Var version.

Section 3 presents the assimilation in the subspace spanned by a single sensitive direction. A particular point concerns the observability of a structure function defined from a posteriori sensitivity. Results with a simple 1D-Var model are presented in section 4 to illustrate the new approach. Section 5 introduces different a posteriori sensitivity structures chosen for this work and results based on *adapted* 3D-Var experiments are described in section 5. Finally, section 6 summarizes the results and presents some conclusions.

2. Flow-dependent structure functions in 3D-Var: The adapted 3D-Var

When representing the background-error covariance matrix $\mathbf{B}$ in a subspace of low dimension with respect to that of the control variable, a regularization term can be added based on the usual 3D-Var covariances with homogenous and isotropic correlations. This can be done in different ways (Fisher 1998; Hamill and Snyder 2000). Here, a variant of the method of Hello and Bouttier (2001) is proposed.

a. 3D variational assimilation

The 3D-Var data assimilation used here has been developed at Environment Canada and is described in Gauthier et al. (1999, 2007). The basic objective of 3D-Var is to obtain the best estimate of the true atmospheric state at the analysis time. In its incremental form, the analysis increment is $\delta\mathbf{x} = \mathbf{x} - \mathbf{x}_b$, where $\mathbf{x}$ is the model state, $\mathbf{x}_b$ is the background state, and $\delta\mathbf{x}$ is obtained by minimizing the cost function:

$$J(\delta\mathbf{x}) = J_b(\delta\mathbf{x}) + J_o(\delta\mathbf{x}) = \frac{1}{2}\delta\mathbf{x}^{\mathrm{T}}\mathbf{B}^{-1}\delta\mathbf{x} + \frac{1}{2}(\mathbf{H}\delta\mathbf{x} - \mathbf{y}')^{\mathrm{T}}\mathbf{R}^{-1}(\mathbf{H}\delta\mathbf{x} - \mathbf{y}'), \quad (1)$$

where $\mathbf{B}$ and $\mathbf{R}$ represent the background and observation error covariance matrices, respectively; $\mathbf{y}' = \mathbf{y} - H(\mathbf{x}_b)$ is the innovation vector; $\mathbf{y}$ the observation vector; and $\mathbf{H}$ is the linearized version of the observation operator H that maps the model state vector $\mathbf{x}$ to observation space. For sake of simplicity, it is assumed that there are no outer iterations. At its minimum, (1) yields the analysis increment $\delta\mathbf{x}_a$ that is added to the background to obtain the analysis $\mathbf{x}_a$ defined as

$$\mathbf{x}_a = \mathbf{x}_b + \delta\mathbf{x}_a = \mathbf{x}_b + \mathbf{K}\mathbf{y}', \quad (2)$$

where $\mathbf{K}$ stands for the Kalman gain matrix expressed as

$$\mathbf{K} = \mathbf{B}\mathbf{H}^{\mathrm{T}}(\mathbf{R} + \mathbf{H}\mathbf{B}\mathbf{H}^{\mathrm{T}})^{-1}. \quad (3)$$

In 3D-Var, the background-error covariances are represented as a stationary matrix. Recently, the assimilation system of Environment Canada has been extended to 4D-Var (Gauthier et al. 2007), in which the background state is compared to the observations at the exact observation time. Moreover in 4D-Var, the background-error statistics are implicitly evolved over the assimilation window, which makes them flow dependent. This slightly relaxes the assumption of stationarity implicit in 3D-Var. In the context of the cycling process of any data assimilation system, it may be important to include a flow-dependent form for the background-error covariances to account for the evolved covariances from the previous assimilation (Fisher and Andersson 2001; Buehner et al. 2010a,b).

b. Adapted 3D-Var approach

To account for anisotropic atmospheric flow, flow dependence can be included in $\mathbf{B}$. The approach at ECMWF has been to explicitly incorporate, within the background-error covariance matrix of 4D-Var, a flow-dependent component defined in a subspace spanned by the leading Hessian singular vectors. This is referred to as a reduced-rank Kalman filter (RRKF; Fisher 1998; Beck and Ehrendorfer 2005). Results demonstrate that the impact of the RRKF is small when the number of Hessian singular vectors used is small compared to the dimension of phase space (Fisher and Andersson 2001).

In the context of 3D-Var, Hello and Bouttier (2001) proposed to estimate the flow-dependent background-error covariances along a single sensitive direction. This approach uses the adjoint-based sensitivities to define the background-error covariance matrix along that component and the stationary background covariances for the remaining orthogonal subspace. As the spatial structure of the analysis increments is driven by the formulation of the background-error covariance, the result is that the analysis increment gives a representation of the sensitivity structure function and its amplitude is determined from the fit to the observations that project in that direction. Otherwise, the analysis increment gives a representation of the stationary background-error covariance matrix commonly used in 3D-Var.

A variant of this approach is proposed here to make corrections to the background along a single sensitive direction. This approach will be referred to as the *adapted 3D-Var*, for which the background-error covariance model embeds the structure functions as defined by sensitivity functions. The new background-error covariance matrix $\tilde{\mathbf{B}}_x$ is composed of the original covariance matrix $\mathbf{B}_h$ with homogeneous and isotropic error correlations to which an additional component is added in the direction spanned by the sensitivity function $\mathbf{f}$. For any given

sensitivity function $\mathbf{f}$, the corresponding *sensitivity structure function* $\mathbf{v}$ is defined as

$$\mathbf{v} = \frac{\mathbf{f}}{\langle \mathbf{f}, \mathbf{f} \rangle_{\mathbf{B}}^{1/2}},$$

where the inner product $\langle \mathbf{f}, \mathbf{f} \rangle_{\mathbf{B}} \equiv \mathbf{f}^{\mathrm{T}} \mathbf{B}_h^{-1} \mathbf{f}$ has been used to normalize $\mathbf{f}$. The new covariance matrix is then

$$\tilde{\mathbf{B}}_x = \mathbf{B}_h + \sigma^2 \mathbf{v}\mathbf{v}^{\mathrm{T}}, \tag{4}$$

with σ^2 the variance added to the background error in the sensitive direction. This assures that the 3D-Var behaves according to $\mathbf{B}_h$ in regions where the sensitivity function vanishes, but adopts the structure of the sensitivity function where it does not.

To formulate the background term in (1) requires the inverse of the covariance matrix $\tilde{\mathbf{B}}_x$. In the appendix, it is shown that

$$\tilde{\mathbf{B}}_x^{-1} = \mathbf{B}_h^{-1/2\mathrm{T}} \left[\mathbf{I} - \frac{\sigma^2}{(\sigma^2 + 1)} (\mathbf{B}_h^{-1/2} \mathbf{v})(\mathbf{B}_h^{-1/2} \mathbf{v})^{\mathrm{T}} \right] \mathbf{B}_h^{-1/2}. \tag{5}$$

When introducing this in (1), it becomes

$$J(\tilde{\boldsymbol{\xi}}) = \frac{1}{2} \tilde{\boldsymbol{\xi}}^{\mathrm{T}} \tilde{\boldsymbol{\xi}} + \frac{1}{2} (\mathbf{H}\mathbf{B}_h^{1/2} \mathbf{L}^{-1} \tilde{\boldsymbol{\xi}} - \mathbf{y}')^{\mathrm{T}} \mathbf{R}^{-1} (\mathbf{H}\mathbf{B}_h^{1/2} \mathbf{L}^{-1} \tilde{\boldsymbol{\xi}} - \mathbf{y}'), \tag{6}$$

where $\mathbf{L}^{-1} = \mathbf{I} + (\sqrt{\sigma^2 + 1} - 1) \tilde{\mathbf{v}} \tilde{\mathbf{v}}^{\mathrm{T}}$ and $\tilde{\mathbf{v}} = \mathbf{B}_h^{-1/2} \mathbf{v}$. Details can be found in the appendix. It can be seen that the standard 3D-Var is retrieved when $\sigma^2 = 0$.

The analysis increment can be expressed as $\delta \mathbf{x}_a = \tilde{\mathbf{K}} \mathbf{y}'$ where the gain matrix $\tilde{\mathbf{K}}$ is

$$\tilde{\mathbf{K}} = \tilde{\mathbf{B}}_x \mathbf{H}^{\mathrm{T}} (\mathbf{R} + \mathbf{H} \tilde{\mathbf{B}}_x \mathbf{H}^{\mathrm{T}})^{-1}. \tag{7}$$

3. Assimilation in the subspace spanned by sensitivities

The motivation for introducing a sensitivity structure in the background covariance is for its potential to impact the most the forecast at a given lead time. In this section, we investigate the case where the background-error covariance contains only that flow-dependent structure. This is the limiting case that reflects the early rationale that comparison to observations would be used to determine the amplitude of the structure having the correct dynamics associated with error growth and at the same time agreeing with the available observations.

a. *Use of a* $\mathbf{B}$ *matrix confined within the subspace spanned by a single sensitive direction*

Assuming that the σ term in (4) does not vanish, we are also interested in the limiting solution when the parameter σ increases. To present the argument, we will take $\mathbf{B}_h = 0$ and the background-error covariance matrix is reduced to its component in the subspace spanned by the sensitivity function and (4) may be written as $\tilde{\mathbf{B}}_x = \sigma^2 \mathbf{v}\mathbf{v}^{\mathrm{T}}$. The analysis increment is then confined to that subspace and can be expressed as

$$\delta \mathbf{x}_a = \tilde{\mathbf{K}} \mathbf{y}' = \alpha \mathbf{v}, \tag{8}$$

and its amplitude α is then found to be

$$\alpha = \frac{(\mathbf{H}\mathbf{v})^{\mathrm{T}} \mathbf{R}^{-1} \mathbf{y}'}{\sigma^{-2} + (\mathbf{H}\mathbf{v})^{\mathrm{T}} \mathbf{R}^{-1} (\mathbf{H}\mathbf{v})} = \frac{\sigma^2 C_1}{1 + \sigma^2 C_2}. \tag{9}$$

The coefficients $C_1 = (\mathbf{H}\mathbf{v})^{\mathrm{T}} \mathbf{R}^{-1} \mathbf{y}'$ and $C_2 = (\mathbf{H}\mathbf{v})^{\mathrm{T}} \mathbf{R}^{-1} (\mathbf{H}\mathbf{v})$ control the magnitude of the analysis increments and depend on several parameters such as the matrix $\mathbf{R}$ of observation error covariances, the estimated innovation, the volume of observations, and also their locations with respect to the amplitude of the sensitive function ($\mathbf{H}\mathbf{v}$). Here, C_1 is the projection of the scaled innovation vector $\mathbf{R}^{-1/2} \mathbf{y}'$ onto the subspace spanned by the sensitivity function and C_2 is the norm of $\mathbf{R}^{-1/2} \mathbf{H}\mathbf{v}$ also scaled with respect to the observation error. If $\mathbf{R}^{-1/2} \mathbf{y}'$ happens to be orthogonal to $\mathbf{R}^{-1/2} (\mathbf{H}\mathbf{v})$, then $C_1 = 0$ and thus $\delta \tilde{\mathbf{x}}_a = \alpha \mathbf{v} = 0$. On the other hand, if $\mathbf{R}^{-1/2} \mathbf{y}'$ happens to be completely in the subspace spanned by the sensitive direction, then $C_1 \neq 0$. Moreover, it is important to point out that the amplitude of the analysis increment (9) will be small if the observation is located in areas of weak sensitivity ($\mathbf{v} \approx 0$) or if the observation value is similar to the background value, even if the observation is located inside an area of strong sensitivity. For large values of σ, the maximum amplitude is given by the ratio C_1/C_2.

This limiting particular case indicates that a single observation should be enough to determine α: the value of α can be determined by a single observation, which would be the true value α_t if the observation were perfect. On the other hand, (9) indicates that when several observations are used, it is the average of the projection of the innovations onto the sensitivity structure that will define the amplitude. This raises the issue of whether the observations are able to detect a particular structure when observation error is present.

Finally, the information content, or degrees of freedom per signal (DFS), corresponds to

$$\mathrm{DFS} = \mathrm{tr}(\mathbf{H}\tilde{\mathbf{K}}) = \frac{\sigma^2 C_2}{1 + \sigma^2 C_2}$$

when $\tilde{\mathbf{B}}_x = \sigma^2\mathbf{v}\mathbf{v}^{\mathrm{T}}$. In the limit $\sigma \to \infty$, DFS $\to 1$, which indicates that when a single direction defines the analysis correction, the degrees of freedom can be reduced by at most 1. Moreover, the analysis increment can be expressed as

$$\delta\mathbf{x}_a = \mathrm{tr}(\mathbf{H}\tilde{\mathbf{K}})\frac{C_1}{C_2}\mathbf{v}.$$

As C_1 represents the projection of the innovations in the direction of $\mathbf{v}$, this shows that information will be added only if the observations can detect the sensitivity structure.

b. Observability of a perturbation structure

To quantify the agreement between the structure function in observation space and the existing observation network, a correlation coefficient ρ is defined as

$$\rho = \frac{(\mathbf{H}\mathbf{v})^{\mathrm{T}}\mathbf{R}^{-1}\mathbf{y}'}{[(\mathbf{H}\mathbf{v})^{\mathrm{T}}\mathbf{R}^{-1}(\mathbf{H}\mathbf{v})]^{1/2}[\mathbf{y}'^{\mathrm{T}}\mathbf{R}^{-1}\mathbf{y}']^{1/2}} = \frac{C_1}{[2C_2J_o(0)]^{1/2}}, \tag{10}$$

where $\mathbf{H}\mathbf{v}$ is the sensitivity structure function in observation space, $\mathbf{y}'$ is the innovation vector, $\mathbf{R}$ is the observation error covariance matrix, and $J_o(0)$ is the observation component of the cost function evaluated before the minimization.

Small values of the correlation coefficient indicate that the structure function does not agree well with the innovation vector. The *observability of a sensitivity structure function* can then be defined as the correlation ρ given by (10). With the assumption that observation errors are uncorrelated, the covariance matrix $\mathbf{R}$ is diagonal and the correlation coefficient can be computed separately for each family of observations. This partition per observation type permits to reveal which data types project the most on a given structure function. In particular, when a single observation is assimilated, the value of the correlation ρ will be equal to 1, unless either $\mathbf{H}\mathbf{v}$ or $\mathbf{y}'$ are exactly null.

In the next section, a simple 1D-Var example is used to illustrate this point.

4. Example based on 1D-Var experiments

A simple one-dimensional (1D) univariate analysis system is used, which is very similar to the one used by Hello and Bouttier (2001) and by Bergot and Doerenbecher (2002). It consists of a circular domain with perimeter of 30 000 km. Within the incremental framework, the cost function is rewritten as in (1) which implies that the background is taken to be null and the observations replaced by the innovation departures $\mathbf{y}'$ with respect to the background. The background-error covariance matrix $\mathbf{B}_h$ in physical space assumes isotropic error correlations in the guess field, with a length scale of 300 km. The observation error covariances are assumed to be uncorrelated with the same observation error variance. Therefore, $\mathbf{R} = \sigma_o^2\mathbf{I}$, where $\mathbf{I}$ is the identity matrix and σ_o^2 is the observation error variance. The sensitive function is represented using simple trigonometric functions as

$$\mathbf{f}(x) = \frac{1}{2}\exp\left[-\frac{1}{2}\left(\frac{x - L/2}{L_b}\right)^2\right]\cos\left[4\left(\frac{x - L/2}{L_b}\right)\right], \tag{11}$$

where L is the length of the circular domain and $L_b = 600$ km is the correlation length scale for $\mathbf{f}$.

The experiments will first try to assess the extent to which a signal of given amplitude can be detected by observations for different levels of observation error. This would correspond to a posteriori sensitivity functions often used to trace back the key analysis errors that can explain forecast error at a given lead time (Klinker et al. 1998; Laroche et al. 2002). So we know after the fact what should be the structure of the correction to the analysis that would impact the forecast the most. The objective is then to use the a posteriori sensitivity as a structure function and find out if the analysis will recover the correct amplitude. In the computation of a posteriori sensitivities no constraint is imposed to have the analysis increment close to the observations.

Taking the background state to be zero and the true state $\mathbf{x}_t = \alpha_t\mathbf{v}$, the background error of this particular realization is then $\varepsilon_b = -\alpha_t\mathbf{v}$. On the other hand, the observation is such that $\mathbf{y} = \mathbf{y}_t + \boldsymbol{\varepsilon}_o = \alpha_t\mathbf{H}\mathbf{v} + \boldsymbol{\varepsilon}_o$ and the background-error covariance matrix is taken as $\tilde{\mathbf{B}}_x = \sigma^2\mathbf{v}\mathbf{v}^{\mathrm{T}}$. The innovation is then $\mathbf{y} - \mathbf{H}\mathbf{x}_b = \alpha_t\mathbf{H}\mathbf{v} + \boldsymbol{\varepsilon}_o$ so that

$$\alpha = \frac{\sigma^2C_2}{1 + \sigma^2C_2}\left[\alpha_t + \frac{(\mathbf{H}\mathbf{v})^{\mathrm{T}}\mathbf{R}^{-1}\boldsymbol{\varepsilon}_o}{(\mathbf{H}\mathbf{v})^{\mathrm{T}}\mathbf{R}^{-1}(\mathbf{H}\mathbf{v})}\right],$$

which expresses the signal α_t with respect to the observation error projected along $\mathbf{v}$. The variance of the noise is $\sigma_\alpha^2 = 1/[(\mathbf{H}\mathbf{v})^{\mathrm{T}}\mathbf{R}^{-1}(\mathbf{H}\mathbf{v})]$ and the signal-to-noise ratio is α_t/σ_α.

To illustrate the impact of the observation error, a posteriori sensitivities have been sampled to generate the observations used in the assimilation. Implicitly, it is assumed then that the amplitude of the sensitivity function is below the level of the background error but greater than that of the observation error so that it can be detected by observations. Assuming $\alpha_t = 2$, Table 1 gives the values of the coefficients C_1 and C_2, and the correlation coefficient ρ for three experiments in which

TABLE 1. Coefficients C_1 and C_2 and correlation coefficient ρ computed using 1D-Var assimilation system for three experiments: (a) perfect observation, (b) $\sigma_o^2 = 1$, and (c) $\sigma_o^2 = 4$. In each case, experiments were done with 10, 20, and 40 observations.

	No. of obs	C_1	C_2	ρ
a) $\mathbf{y}' = 2(\mathbf{Hv})$	10	1.29	0.64	0.99
	20	1.96	0.97	0.99
	40	2.26	1.13	1
b) $\mathbf{y}' = 2(\mathbf{Hv}) + \boldsymbol{\varepsilon}_o$	10	0.95	0.64	0.38
	20	1.15	0.97	0.22
	40	1.48	1.13	0.20
c) $\mathbf{y}' = 2(\mathbf{Hv}) + \boldsymbol{\varepsilon}_o$	10	0.89	0.64	0.17
	20	0.89	0.97	0.11
	40	0.87	1.13	0.08

the observation is first taken to be the truth and then when random observation error is added with variance $\sigma_o^2 = 1$ and 4, respectively. In all three cases, experiments were done with 10, 20, and 40 observations at different locations, to improve the sampling of the structure of the signal. With perfect observations, the amplitude is recovered and the correlation is very close to 1. Adding an observation error dramatically reduces the correlation. With $\sigma_o^2 = 1$, the correlation decreases with the number of observations. Increasing the observation error to a level that compares with the signal, there is no correlation at all between the analysis increment and the sensitivity function. Figure 1 shows the amplitude of the analysis increment as a function of σ for these experiments. When $\sigma_o^2 = 1$, the amplitude is less than the actual value that reflects the fact that the presence of random error "blurs" the signal.

As studied in Hello and Bouttier (2001) and Bergot and Doerenbecher (2002), a single observation should be enough to determine the amplitude of the correction, provided this observation projects onto the sensitivity structure ($C_1 \neq 0$). However, if an observation error is present, then the analysis would also fit the observation error. This would happen when $\sigma^2 \to \infty$. With more observations and with no observation error, all observations would agree on what α should be; but if the observation error is above the signal, α would vary randomly and the overall fit should yield a value near zero. This is what Fig. 1 indicates.

In those previous experiments, the background-error covariance used a sensitivity structure function that corresponded exactly to what was observed. However, the sensitivities are computed under a number of assumptions and this may result in differences in sensitivities present in the atmosphere and detected by the observations from those being computed with a given numerical model (referred to as $\mathbf{v}_t$). In a second set of experiments, different structure functions were used in the background term and to generate the observations. In these experiments, the observations were generated by introducing

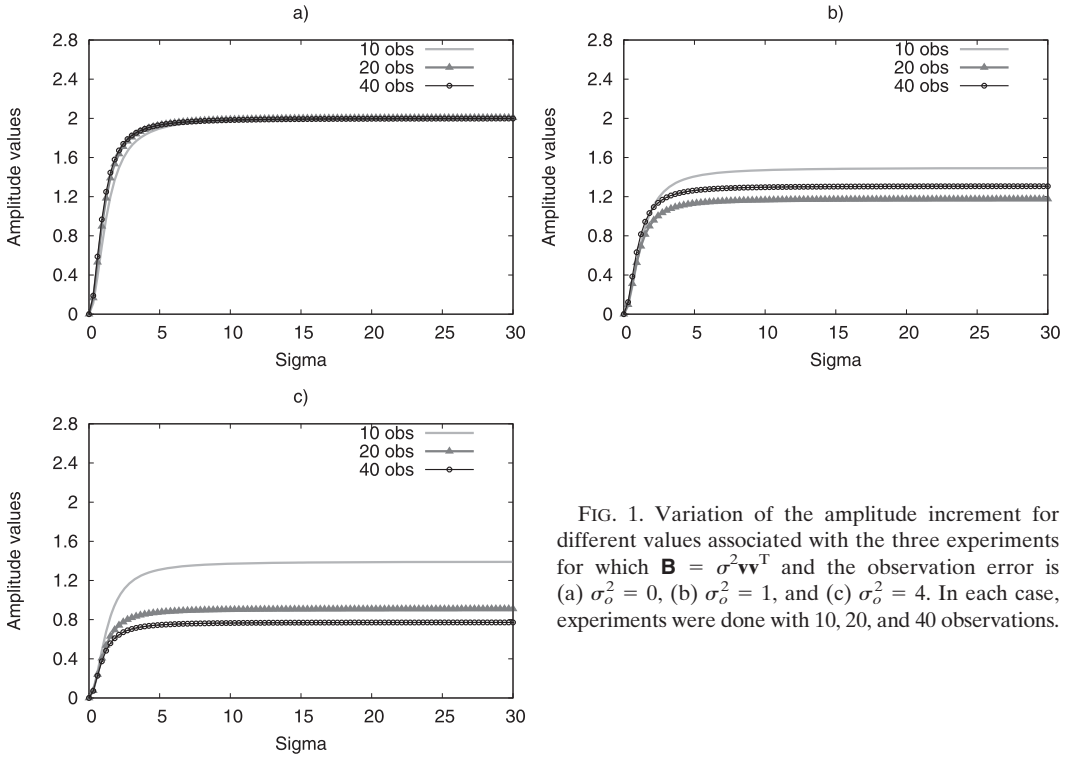

FIG. 1. Variation of the amplitude increment for different values associated with the three experiments for which $\mathbf{B} = \sigma^2\mathbf{v}\mathbf{v}^{\mathrm{T}}$ and the observation error is (a) $\sigma_o^2 = 0$, (b) $\sigma_o^2 = 1$, and (c) $\sigma_o^2 = 4$. In each case, experiments were done with 10, 20, and 40 observations.

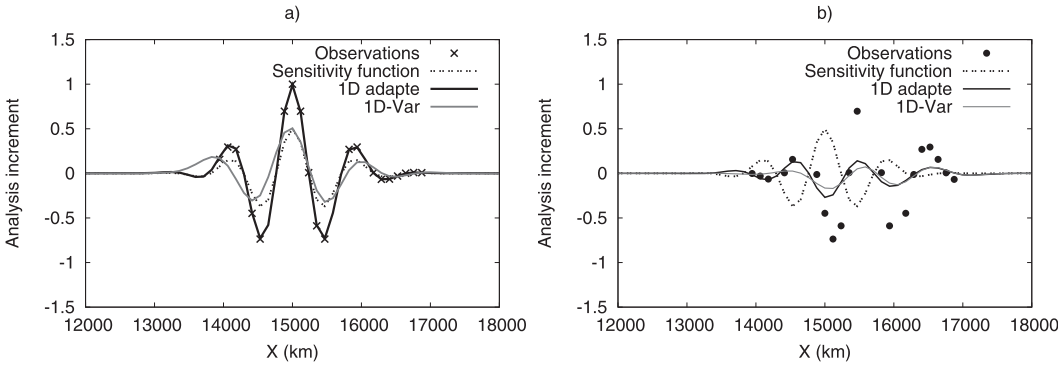

FIG. 2. Analysis increments obtained with an adapted 1D-Var (black) and a standard 1D-Var (gray). The sensitivity function used in the analysis is also shown (dotted line). The observations are shown as crosses or dots for the two experiments. In all cases, the adapted 1D-Var used $\sigma = 10$: the observations were generated (a) by sampling the sensitivity structure function used in the analysis and (b) from a function corresponding to a different structure function.

a phase shift in the structure function. The results are shown in Fig. 2. When the observations are sampled from $\mathbf{v} = \mathbf{v}_t$, Fig. 2a shows that the adapted 1D-Var does recover the right amplitude. In Fig. 2b, $\mathbf{v} \neq \mathbf{v}_t$ and the observations have contradicting views on what the amplitude of $\mathbf{v}$ should be, and with several observations, the net result is an average of the individual contributions and the amplitude of the analysis increment is then very small. Figure 2 also shows, in gray, the analysis increment obtained with the standard 1D-Var (homogeneous correlations). It shows that the standard 1D-Var needs several observations to reconstruct the signal. By opposition, the adapted 1D-Var would be able to reconstruct the correct increment from a single observation provided $\mathbf{v} = \mathbf{v}_t$ when there is no observation error. If not, the adapted 1D-Var with several observations tends to yield an increment of small amplitude.

In summary, a 1D-Var example was used to show that, in the presence of observation error and with several observations, the adapted 1D-Var can recover the signal, provided the observation error is smaller than the signal. If the sensitivity structure functions differ from those present in the atmosphere and detected by the observations, the adapted 1D-Var will underestimate the amplitude of the signal. In the next section, an adapted 3D-Var was implemented within the variational system of Environment Canada and experiments have been carried out to test if the added flow-dependent structure function manages to improve the forecasts.

5. Results with 3D-Var using different definitions for the structure functions

A posteriori sensitivities have a structure and amplitude that result in a significant reduction in the forecast error. However, they are not constrained to fit the observations at the initial time (Isaksen et al. 2005). In this section, sensitivity structure functions are defined as normalized a posteriori sensitivities. The object is then to investigate the extent to which the assimilated observations can recover the amplitude of the a posteriori sensitivity. There are different ways to define the a posteriori sensitivities. The sensitivities depend on the metric used to measure the forecast error (e.g., dry energy norm, Hessian norm, etc.). The definition of norm may also involve the area over which it is computed. When the sensitivity function is computed globally, this defines a global sensitivity function. Local sensitivity functions can be also calculated to identify the source of forecast error only over a local area (Hello and Bouttier 2001). By computing the forecast error over a limited area, the local sensitivity function focuses in changes in the initial conditions that will impact that specific area at a given lead time. In Caron et al. (2007b), the computation of sensitivity functions was done by imposing also a nonlinear balance constraint using a potential vorticity (PV) inversion method. Finally, it is important to remember that the sensitivities, as for singular vectors, depend on the resolution and configuration of the adjoint model (e.g., simplified physics, vertical extent, and resolution). This leads to several possibilities to consider as potential sensitivity structure functions.

Several experiments in which different definitions of the sensitivity functions were used as structure functions in an adapted 3D-Var based on the operational 3D-Var of Environment Canada (Gauthier et al. 1999, 2007). Experiments involving winter cases documented by Caron et al. (2007a) will be discussed. Key analysis errors were estimated for four 3D-Var analyses: at 1200 UTC 6 January and 27 January 2003, at 0000 UTC 19 January 2002, and at 1200 UTC 6 February 2002. Those cases were associated with cases of severe weather over North America.

TABLE 2. Correlation coefficient computed for different data types and for all observations combined. Different sensitivity functions from the key analysis error algorithm are used: GLOBAL (initial corrections that minimized the 24-h forecast error over the globe), LOCAL (initial corrections that minimized the 24-h forecast error over an area on the east coast of North America), HEMISPHERIC (initial corrections over the latitudinal band 25°–90°N), and PV-bal (balanced initial corrections over the latitudinal band 25°–90°N). Cases shown are (a) 27 Jan 2003, (b) 6 Jan 2003, (c) 6 Feb 2002, and (d) 19 Jan 2002.

		Correlation coef ρ			
Structure functions	Obs type	27 Jan 2003	6 Jan 2003	6 Feb 2002	19 Jan 2002
Global function	Raob	0.01	0.02	0.03	−0.01
	AIREP	0.00	0.02	−0.01	−0.01
	AMV	0.02	0.01	0.02	0.02
	SURFC	0.14	0.11	0.19	0.04
	ATOVS	0.13	0.11	0.07	0.12
	TOTAL	0.05	0.05	0.05	0.03
Local function	Raob	−0.01	0.0	−0.01	−0.02
	AIREP	−0.03	−0.01	−0.03	−0.03
	AMV	0	0.03	−0.04	0.0
	SURFC	0.04	−0.03	0	0.02
	ATOVS	0.05	0.01	0.06	0.02
	TOTAL	0.0	0.0	0.0	−0.01
Hemispheric function	Raob	0.00	0.02	0.01	0.01
	AIREP	−0.05	0.02	−0.02	−0.03
	AMV	−0.05	−0.08	−0.02	0.02
	SURFC	0.12	0.1	0.16	0.08
	ATOVS	0.08	0.07	0.07	0.04
	TOTAL	0.03	0.04	0.04	0.02
PV-bal function	Raob	0.01	0.0	0.01	0.0
	AIREP	−0.03	0.01	−0.03	0.0
	AMV	−0.04	−0.08	−0.03	0.01
	SURFC	0.04	−0.06	0.21	0.06
	ATOVS	0.09	0.08	0.08	0.05
	TOTAL	0.03	−0.01	0.06	0.02

For all cases, a posteriori sensitivities were computed in different ways to minimize the 24-h forecast error as measured with respect to a verifying analysis. The method employed is explained in Laroche et al. (2002) and Caron et al. (2007a). Four types of structure functions will be considered in our study:

- a global sensitivity, for which the error is measured globally,
- a local sensitivity, for which the error is measured over an area on the east coast of North America,
- a hemispheric sensitivity function computed over the latitudinal band 25°–90°N,
- a sensitivity function, for which the control variable is potential vorticity (PV), which constrains the sensitivity to be more dynamically balanced, hereinafter called PV-bal (Caron et al. 2007b).

All cases used the dry energy norm at initial and end time. As already mentioned, the analysis increment (9) has the direction of the sensitivity structure function and the amplitude that best fits the observations. Table 2 summarizes the correlation associated with different observation types for all four cases. The results show poor correlations between the observations and the sensitivity functions in observation space. This indicates that in the limiting case where $\sigma \to \infty$, the adapted 3D-Var could not be expected to improve the forecast as much as the key analyses do. This is true for all cases considered here.

a. A test case

For each case documented in Caron et al. (2007a), regular 3D-Var global analyses were performed using the full set of observations assimilated operationally at Environment Canada and the background state is the same that was used in the 3D-Var system operational at the time. For each case, the analysis increment is as close as possible to the true atmospheric state in a root-mean-square sense. To test the adapted 3D-Var, analysis increments obtained from 3D-Var analyses were normalized with respect to the norm $\langle \mathbf{f}, \mathbf{f} \rangle_{\mathbf{B}}$ defined in section 2b and used as the structure function $\mathbf{v}$ in $\tilde{\mathbf{B}}_x = \sigma^2 \mathbf{v}\mathbf{v}^{\mathrm{T}}$. In that case, the objective was to test whether this limiting case of the adapted 3D-Var could recover the amplitude of the analysis increment, knowing that this structure does have the ability to fit the observations. Figure 3 shows the estimated amplitude of the analysis increment calculated from (9) as a function of the parameter σ for different families of observational data. The estimated

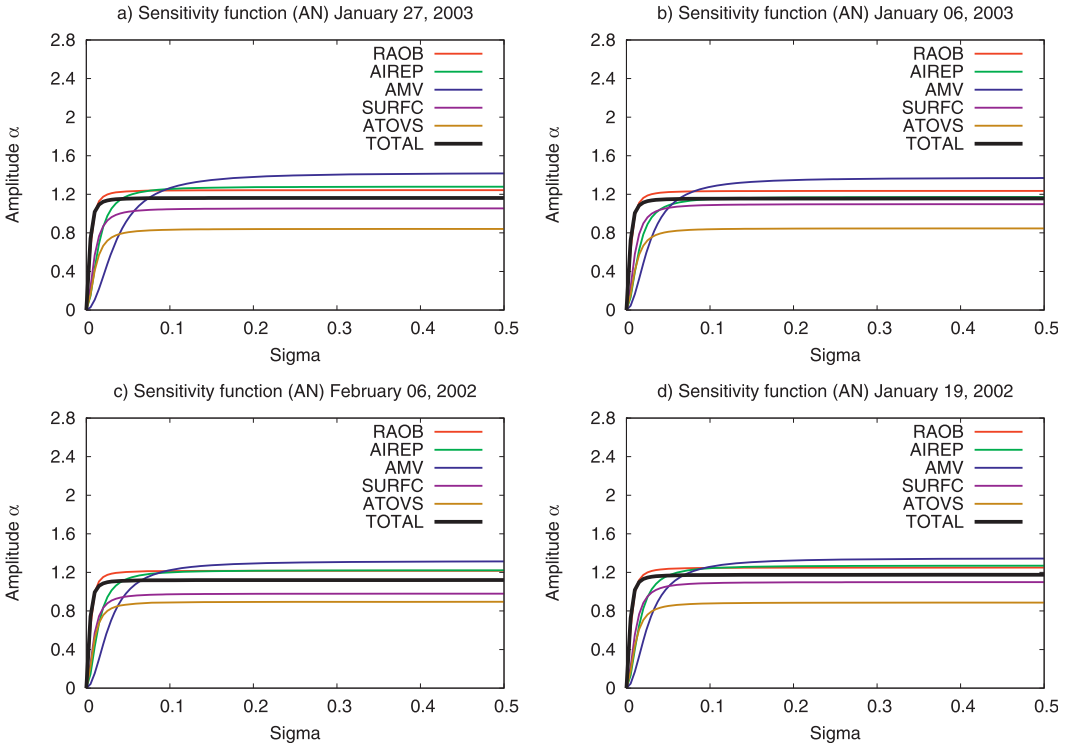

FIG. 3. Amplitude of the analysis increment as a function of parameter σ for different families of observational data: raob, AIREP, AMVs, SURFC, radiance data from satellites (ATOVS), and all observations combined (TOTAL). The 3D-Var analyses are used as sensitivity function to adapt the background-error covariance matrix for 4 case studies: (a) 27 Jan 2003, (b) 6 Jan 2003, (c) 6 Feb 2002, and (d) 19 Jan 2002.

amplitude of analysis increment increases rapidly with σ and saturates for each data types at a value corresponding to the ratio C_1/C_2. This example indicates that the adapted 3D-Var analysis increment recovers the amplitude of the sensitive function when σ is sufficiently large. To assess the agreement between the analysis increment for each case and the observation network, the correlation coefficients have been computed for all data types and the results are summarized in Table 3. The correlation coefficients values are shown for each family of observations and all observations combined indicate good agreement for all cases.

b. *Application in an adapted 3D-Var context*

The adapted 3D-Var is closer to the observations than the 3D-Var for observed storm cases documented in Caron et al. (2007a). A measure of the fit to the observations is given by the observation component of the cost function J_o. Following Caron et al. (2007a), the relative difference in J_o is examined individually for each family of observations [radiosondes (raob), aircraft report (AIREP), surface and ship data (SURFC), radiances data from satellite: Advanced Television and Infrared Observation Satellite (TIROS) Operational Vertical Sounder (ATOVS), and wind vectors derived from satellite data: atmospheric motion vectors (AMVs)] and for the combined set of observations combined (TOTAL), in the form

$$\Delta J_o = \frac{J_o(\mathbf{x}^{\mathrm{Ad.3D}}) - J_o(\mathbf{x}^{\mathrm{3D}})}{J_o(\mathbf{x}^{\mathrm{3D}})}, \tag{12}$$

where $J_o(\mathbf{x}) = 1/2(\mathbf{y} - \mathbf{Hx})^{\mathrm{T}}\mathbf{R}^{-1}(\mathbf{y} - \mathbf{Hx})$ measures the distance between the model state $\mathbf{x}$ and the observations $\mathbf{y}$. A positive value $[J_o(\mathbf{x}^{\mathrm{Ad.3D}}) > J_o(\mathbf{x}^{\mathrm{3D}})]$ means

TABLE 3. Correlation coefficient computed for different data types and for all observations combined. The 3D-Var analyses are used as sensitivity function to adapt the background-error covariance matrix for 4 case studies: (a) 27 Jan 2003, (b) 6 Jan 2003, (c) 6 Feb 2002, and (d) 19 Jan 2002.

	Correlation coef ρ			
Obs type	27 Jan 2003	6 Jan 2003	6 Feb 2002	19 Jan 2002
Raob	0.73	0.76	0.77	0.76
AIREP	0.73	0.73	0.73	0.72
AMV	0.68	0.72	0.72	0.73
SURFC	0.69	0.74	0.75	0.76
ATOVS	0.59	0.58	0.71	0.65
TOTAL	0.71	0.73	0.75	0.74

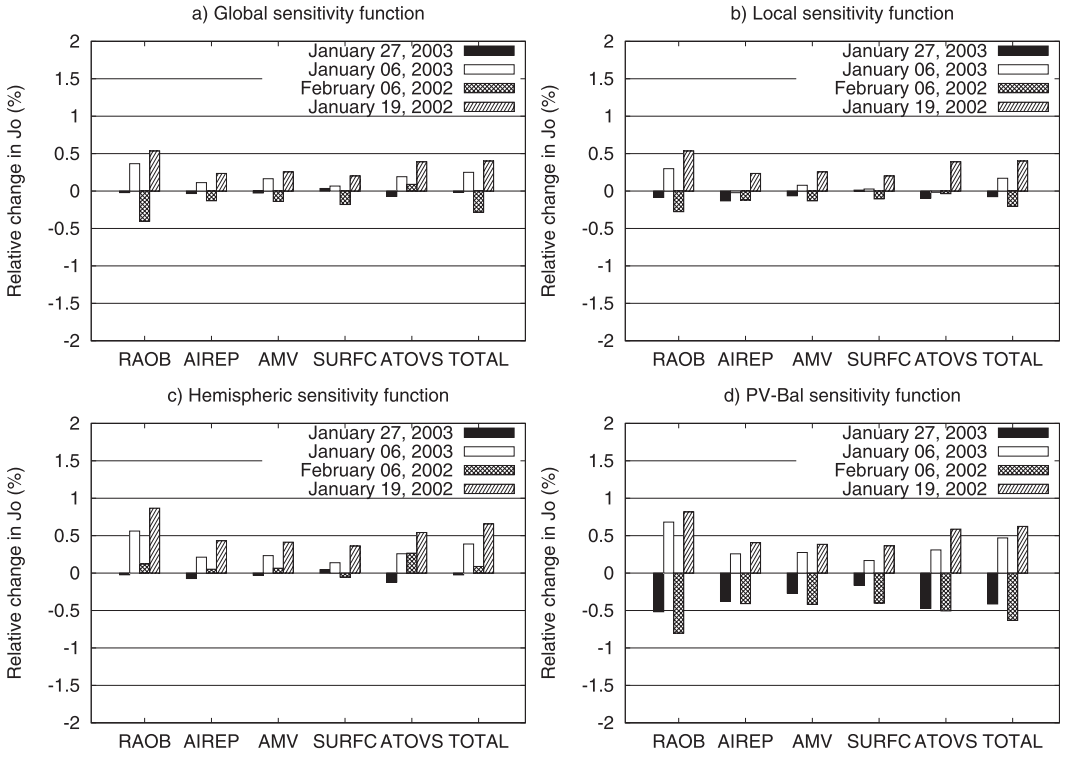

FIG. 4. Relative change in the global fit to the observations for different families of observational data. The a posteriori sensitivity functions are used as structure functions in the adapted 3D-Var for four case studies. A positive value means that the adapted 3D-Var analyses are farther away from the observations than the operational analysis and a negative value means that the adapted 3D-Var analyses fit the observation values better than 3D-Var.

that that the adapted 3D-Var analyses are farther away from the observations than the corresponding operational analysis and, conversely, a negative value $[J_o(\mathbf{x}^{\mathrm{Ad.3D}}) < J_o(\mathbf{x}^{\mathrm{3D}})]$ means that the adapted 3D-Var analyses fit the observations better than 3D-Var.

As demonstrated by Caron et al. (2007a,b), adjoint sensitivity structures from the Canadian Meteorological Centre (CMC) energy-norm-based key analysis error algorithm manage to minimize short-range (24 h) forecast errors, but depart more from the observations than the original 3D-Var analysis. The percentage of improvement or degradation of the fit to the observations is shown in Fig. 4 when a posteriori sensitivities are used as structure functions in the adapted 3D-Var. The results show that the experiments with different ways to define sensitivity functions can lead to quite different results. However, for the cases presented here the results are approximately neutral.

c. *Experiments with a pseudoinverse defined in a subspace spanned by a finite number of singular vectors*

For true flow-dependent background-error covariances, a priori structure functions would be defined either as a finite number of singular vectors (Leutbecher 2003) or from the sensitivity gradient that identifies those structures that would impact the most the forecast as measured by a given metric (Hello and Bouttier 2001). Here, the question asked is to know whether those structures can both fit the observations and reduce the forecast error.

The SVs are the perturbations with the largest amplification rate over a given time interval. A set of 60 singular vectors was calculated for 18 cases of December 2007 for a time interval of 48 h. The singular vectors are calculated using the total energy norm at initial and final times. The first singular vector (SV_1) has the largest singular value that is much larger than the others. The correlation coefficients values in Table 4, suggest that the SV_1 at initial and final time does not correlate well with the innovation vector. The pseudoinverse is the perturbation with the largest impact on the forecast error (Mahidjiba et al. 2007) obtained by expressing the forecast error at 48 h as a linear combination of a finite number of singular vectors. Using here the set of 60 singular vectors, this leads to a correction to the initial conditions that does reduce the forecast error represented in a subspace that truly represents the growing modes

TABLE 4. Correlation coefficient computed for all data types for 18 cases of December 2007. The first singular vector at initial and final time and the pseudoinverse are used as structure functions.

Date	Obs. type	Correlation coef ρ		
		SV No. 1 initial time	SV No. 1 final time	Pseudoinverse
0000 UTC 1 Dec 2007	TOTAL	0.0098	0.0067	0.0169
1200 UTC 2 Dec 2007	TOTAL	0.0140	−0.0179	−0.0011
0000 UTC 4 Dec 2007	TOTAL	−0.0187	−0.0211	−0.0034
1200 UTC 5 Dec 2007	TOTAL	0.0022	−0.0020	0.0124
0000 UTC 7 Dec 2007	TOTAL	0.0159	0.0020	−0.0033
1200 UTC 8 Dec 2007	TOTAL	0.0019	0.0212	0.0062
0000 UTC 10 Dec 2007	TOTAL	−0.0029	−0.0151	0.0040
1200 UTC 11 Dec 2007	TOTAL	0.0054	0.0148	0.0096
0000 UTC 13 Dec 2007	TOTAL	0.0125	−0.0241	−0.0028
1200 UTC 14 Dec 2007	TOTAL	0.0224	−0.056	0.0209
0000 UTC 16 Dec 2007	TOTAL	0.0125	0.0235	0.0234
1200 UTC 17 Dec 2007	TOTAL	0.0041	0.0465	−0.0064
0000 UTC 19 Dec 2007	TOTAL	0.0119	−0.0097	−0.0010
1200 UTC 20 Dec 2007	TOTAL	0.0067	0.0217	0.0047
0000 UTC 22 Dec 2007	TOTAL	0.0103	−0.0084	−0.0053
1200 UTC 23 Dec 2007	TOTAL	0.0099	−0.0068	0.0110
0000 UTC 25 Dec 2007	TOTAL	−0.0020	−0.0065	−0.0059
1200 UTC 26 Dec 2007	TOTAL	−0.0086	0.0056	−0.0117

of forecast error. However, the last column of Table 4 indicates that this pseudoinverse is not well correlated with the observations either: the correlation coefficient is no better than that of the first singular vector alone. We therefore conclude that the structures defined by singular vectors are not well correlated with observations, which means that they are not observable given the level of error in the observations being assimilated. Of course, different factors influence the definition a singular vector: metric used at the initial and final time, characteristics of the tangent-linear and adjoint model used, and other factors. Our experiments only cover a single example and it would be worth investigating if these factors can lead to more observable singular vectors. This is beyond the scope of the present study.

6. Summary and conclusions

The argument presented in this paper is that structures that can explain a substantial part of future error growth have a small amplitude and the signal is often below the level of observation error. In other words, the signal-to-noise ratio is too low for them to be detected by observations. This is an important issue for the use of flow-dependent structures that could be related to precursors of error growth. Several experiments have been performed to include known a posteriori sensitivities as structure functions within a so-called adapted 3D-Var. The results obtained by Caron et al. (2007a,b) and in our own experiments indicate that a posteriori key analyses do succeed to significantly reduce the forecast error, but tend to pull the analysis further away from the observations than the reference analysis they were correcting. The experiments with an adapted 3D-Var manage to correct the analysis with the structure of the key analysis under the constraint that the resulting analysis is close to the observations. The results indicate that the analysis is then close to the observations, but this does not significantly improve the quality of the forecast. Pushing this to the limit where the bulk of the forecast error variance is put in the direction of the sensitivity structure function, it was expected that one would recover the amplitude of the a posteriori sensitivity (or key analysis). This was not the case. A close study of this limiting case indicated that the retrieved amplitude is determined by the correlation of the structure function with the innovations. With a single observation, one recovers the projection of the innovation in that direction; but adding more observations results in very small amplitude, as the correlation of the innovation vector with the image, in observation space, of the sensitivity structure function is small.

The Langland and Baker (2004, hereafter noted as LB04) method is projecting the analysis correction onto the structures that should influence the most the forecast. This is in essence the same thing as what the singular vectors are aiming for using the adjoint model to identify those structures that influence the most the forecast at a given lead time. In many studies that used the LB04 method, it was found that the impact of individual observations could be positive. In fact, it was found that only a little more than half of the observations had a positive impact on the forecast. In view of our results, this

seems to indicate that the signal is at the noise level and can barely be detected by the available observations.

These results are important and more thought is needed on how to include information about precursors in the analysis. An element that needs to be considered is that the analysis may have to wait for the instability to develop above the signal-to-noise ratio for the observations to be able to detect it and properly correct the initial conditions. In a sense, this would indicate that evolved covariances obtained from a Kalman filter as obtained from an ensemble Kalman filter (Houtekamer et al. 2009) should be better observable than covariances represented in a subspace spanned by singular vectors. However, evolved singular vectors could be a good prospect. This will be the object of future work.

Acknowledgments. Authors would like to deeply thank Dr. Jean-François Caron who provided the a posteriori sensitivity functions used in this study. Stimulating discussions with Drs. Mark Buehner and Ahmed Mahidjiba were very helpful during the course of this study. They kindly provided the singular vectors and the pseudoinverses used in this study. Environment Canada provided the computing facilities, and technical assistance for the use of their assimilation system.

This work has been funded mostly by Grant 500-B of the Canadian Foundation for Climate and Atmospheric Sciences (CFCAS) for the project on the *Impact of Observing Systems on Forecasting Extreme Weather in the Short, Medium and Extended Range: A Canadian Contribution to THORPEX*, with additional support from Discovery Grant 357091 of the Natural Sciences and Engineering Research Council (NSERC) of Canada.

APPENDIX

Formulation of the Adapted 3D-Var

Adding a sensitive component to $\mathbf{B}_h$ led to

$$\tilde{\mathbf{B}}_x = \mathbf{B}_h + \sigma^2 \mathbf{v}\mathbf{v}^{\mathrm{T}},$$

where $\langle \mathbf{v}, \mathbf{v} \rangle_{\mathbf{B}} \equiv \mathbf{v}^{\mathrm{T}}\mathbf{B}_h^{-1}\mathbf{v} = 1$. Using the Sherman–Morrison formula (Golub and Van Loan 1996), the inverse of $\tilde{\mathbf{B}}_x$ is found to be

$$\tilde{\mathbf{B}}_x^{-1} = \mathbf{B}_h^{-1/2\mathrm{T}}\left[\mathbf{I} - \frac{\sigma^2}{(\sigma^2+1)}(\mathbf{B}_h^{-1/2}\mathbf{v})(\mathbf{B}_h^{-1/2}\mathbf{v})^{\mathrm{T}}\right]\mathbf{B}_h^{-1/2} \tag{A1}$$

and the 3D-Var cost function (1) can be rewritten as

$$J(\delta\mathbf{x}) = \frac{1}{2}\delta\mathbf{x}^{\mathrm{T}}\mathbf{B}_h^{-1/2\mathrm{T}}\left[\mathbf{I} - \frac{\sigma^2}{(\sigma^2+1)}(\mathbf{B}_h^{-1/2}\mathbf{v})(\mathbf{B}_h^{-1/2}\mathbf{v})^{\mathrm{T}}\right] \times \mathbf{B}_h^{-1/2}\delta\mathbf{x} + \frac{1}{2}(\mathbf{H}\delta\mathbf{x} - \mathbf{y}')^{\mathrm{T}}\mathbf{R}^{-1}(\mathbf{H}\delta\mathbf{x} - \mathbf{y}').$$

Defining the change of variables, $\boldsymbol{\xi} = \mathbf{B}_h^{-1/2}\delta\mathbf{x}$ and $\tilde{\mathbf{v}} = \mathbf{B}_h^{-1/2}\mathbf{v}$ yields

$$J(\boldsymbol{\xi}) = \frac{1}{2}\boldsymbol{\xi}^{\mathrm{T}}\left(\mathbf{I} - \frac{\sigma^2}{\sigma^2+1}\tilde{\mathbf{v}}\tilde{\mathbf{v}}^{\mathrm{T}}\right)\boldsymbol{\xi} + \frac{1}{2}(\mathbf{H}\mathbf{B}_h^{1/2}\boldsymbol{\xi} - \mathbf{y}')^{\mathrm{T}} \times \mathbf{R}^{-1}(\mathbf{H}\mathbf{B}_h^{1/2}\boldsymbol{\xi} - \mathbf{y}') = J_b(\boldsymbol{\xi}) + J_o(\boldsymbol{\xi}). \tag{A2}$$

So defined, the sensitivity structure function is such that

$$\tilde{\mathbf{v}}^{\mathrm{T}}\tilde{\mathbf{v}} = \mathbf{v}^{\mathrm{T}}\mathbf{B}_h^{-1/2}\mathbf{B}_h^{-1/2}\mathbf{v} = \mathbf{v}^{\mathrm{T}}\mathbf{B}_h^{-1}\mathbf{v} = 1.$$

In terms of these new variables, we have

$$\left(\mathbf{I} - \frac{\sigma^2}{\sigma^2+1}\tilde{\mathbf{v}}\tilde{\mathbf{v}}^{\mathrm{T}}\right) = \left[\mathbf{I} + \frac{(\sqrt{\sigma^2+1} - \sigma^2 - 1)}{\sigma^2+1}\tilde{\mathbf{v}}\tilde{\mathbf{v}}^{\mathrm{T}}\right]^2 = \mathbf{L}^{\mathrm{T}}\mathbf{L},$$

with

$$\mathbf{L} = \mathbf{I} + \left(\frac{\sqrt{\sigma^2+1} - \sigma^2 - 1}{\sigma^2+1}\right)\tilde{\mathbf{v}}\tilde{\mathbf{v}}^{\mathrm{T}} = \mathbf{L}^{\mathrm{T}}. \tag{A3}$$

This allows us to introduce another change of variable $\boldsymbol{\xi} = \mathbf{L}\tilde{\boldsymbol{\xi}}$, so that $\tilde{\boldsymbol{\xi}} = \mathbf{L}^{-1}\boldsymbol{\xi}$. The inverse of $\mathbf{L}$ is found to be

$$\mathbf{L}^{-1} = \mathbf{I} + (\sqrt{\sigma^2+1} - 1)\tilde{\mathbf{v}}\tilde{\mathbf{v}}^{\mathrm{T}},$$

so that (A2) is finally expressed as

$$J(\tilde{\boldsymbol{\xi}}) = \frac{1}{2}\tilde{\boldsymbol{\xi}}^{\mathrm{T}}\tilde{\boldsymbol{\xi}} + \frac{1}{2}(\mathbf{H}\mathbf{B}_h^{1/2}\mathbf{L}^{-1}\tilde{\boldsymbol{\xi}} - \mathbf{y}')^{\mathrm{T}}\mathbf{R}^{-1}(\mathbf{H}\mathbf{B}_h^{1/2}\mathbf{L}^{-1}\tilde{\boldsymbol{\xi}} - \mathbf{y}'). \tag{A4}$$

Its gradient is readily found to be

$$\nabla_{\tilde{\boldsymbol{\xi}}} J = \tilde{\boldsymbol{\xi}} + \mathbf{L}^{-\mathrm{T}}\mathbf{B}_h^{1/2}\mathbf{H}^{\mathrm{T}}\mathbf{R}^{-1}(\mathbf{H}\mathbf{B}_h^{1/2}\mathbf{L}^{-1}\tilde{\boldsymbol{\xi}} - \mathbf{y}').$$

REFERENCES

Beck, A., and M. Ehrendorfer, 2005: Singular-vector-based covariance propagation in a quasigeostrophic assimilation system. *Mon. Wea. Rev.,* **133,** 1295–1310.

Bergot, T., and A. Doerenbecher, 2002: A study on the optimization of the deployment of targeted observations using adjoint-based methods. *Quart. J. Roy. Meteor. Soc.,* **128,** 1689–1712.

Berre, L., G. Desroziers, L. Raynaud, R. Montroty, and F. Gibier, 2009: Consistent operational ensemble variational assimilation. *Proc. CAWCR Workshop on Ensemble Prediction and*

Data Assimilation, Melbourne, Australia, Australian Bureau of Meteorology, Paper 196, 8 pp.

Buehner, M., P. L. Houtekamer, C. Charette, H. L. Mitchell, and B. He, 2010a: Intercomparaison of variational data assimilation and ensemble Kalman filter for global deterministic NWP. Part I: Description and single-observation experiments. *Mon. Wea. Rev.,* **138,** 1550–1566.

——, ——, ——, ——, and ——, 2010b: Intercomparaison of variational data assimilation and ensemble Kalman filter for global deterministic NWP. Part II: One-month experiments with real observations. *Mon. Wea. Rev.,* **138,** 1567–1586.

Buizza, R., J.-R. Bidlot, N. Wedi, M. Fuentes, M. Hamrud, G. Holt, and F. Vitart, 2007a: The new ECMWF VAREPS (Variable Resolution Ensemble Prediction System). *Quart. J. Roy. Meteor. Soc.,* **133,** 681–695.

——, C. Cardinali, G. Kelly, and J.-N. Thépaut, 2007b: The value of observations. II: The value of observations located in singular-vector-based target areas. *Quart. J. Roy. Meteor. Soc.,* **133,** 1817–1832.

Cardinali, C., R. Buizza, G. Kelly, M. Shapiro, and J.-N. Thépaut, 2007: The value of observations. III: Influence of weather regimes on targeting. *Quart. J. Roy. Meteor. Soc.,* **133,** 1833–1842.

Caron, J.-F., M. K. Yau, S. Laroche, and P. Zwack, 2007a: The characteristics of key analysis errors. Part I: Dynamical balance and comparison with observations. *Mon. Wea. Rev.,* **135,** 249–266.

——, ——, ——, and ——, 2007b: The characteristics of key analysis errors. Part II: The importance of the PV corrections and the impact of balance. *Mon. Wea. Rev.,* **135,** 267–280.

Evensen, G., 1994: Sequencial data assimilation with a nonlinear quasi-geostrophic model using Monte Carlo methods to forecast error statistics. *J. Geophys. Res.,* **99,** 10 143–10 162.

Fisher, M., 1998: Development of a simplified Kalman Filter. ECMWF Research Department Tech. Memo. 260, ECMWF, 16 pp.

——, and E. Andersson, 2001: Developments in 4D-Var and Kalman filtering. ECMWF Research Department Tech. Memo. 347, ECMWF, 36 pp.

Gauthier, P., C. Charette, L. Fillion, P. Koclas, and S. Laroche, 1999: Implementation of a 3D variational data assimilation system at the Canadian Meteorological Centre. Part I: The global analysis. *Atmos.–Ocean,* **37,** 103–156.

——, M. Tanguay, S. Laroche, S. Pellerin, and J. Morneau, 2007: Extension of 3DVAR to 4DVAR: Implementation of 4DVAR at the Meteorological Service of Canada. *Mon. Wea. Rev.,* **135,** 2339–2354.

Golub, H. G., and C. F. Van Loan, 1996: *Matrix Computations*. 3rd ed. The John Hopkins University Press, 694 pp.

Hamill, T., and C. Snyder, 2000: A hybrid ensemble Kalman filter–3D variational analysis scheme. *Mon. Wea. Rev.,* **128,** 2905–2919.

Hello, G., and F. Bouttier, 2001: Using adjoint sensitivity as a local structure function in variational data assimilation. *Nonlinear Processes Geophys.,* **8,** 347–355.

——, F. Lalaurette, and J.-N. Thépaut, 2000: Combined use of sensitivity information and observations to improve meteorological forecasts: A feasibility study applied to the 'Christmas storm' case. *Quart. J. Roy. Meteor. Soc.,* **126,** 621–647.

Houtekamer, P. L., H. L. Mitchell, and X. Deng, 2009: Model error representation in an operational ensemble Kalman filter. *Mon. Wea. Rev,* **137,** 2126–2143.

Isaksen, L., M. Fisher, E. Andersson, and J. Barkmeijer, 2005: The structure and realism of sensitivity perturbations and their interpretation as ''Key analysis errors.'' *Quart. J. Roy. Meteor. Soc.,* **131,** 3053–3078.

Joly, A., and Coauthors, 1999: Overview of the field phase of the Fronts and Atlantic Storm Track Experiment (FASTEX) project. *Quart. J. Roy. Meteor. Soc.,* **125,** 3131–3164.

Kelly, G., J.-N. Thépaut, R. Buizza, and C. Cardinali, 2007: The value of observations. I: Data denial experiments for the Atlantic and the Pacific. *Quart. J. Roy. Meteor. Soc.,* **133,** 1803–1815.

Klinker, E., F. Rabier, and R. Gelaro, 1998: Estimation of key analysis errors using the adjoint technique. *Quart. J. Roy. Meteor. Soc.,* **124,** 1909–1933.

Lacarra, J. F., and O. Talagrand, 1988: Short-range evolution of small perturbations in a barotropic model. *Tellus,* **40A,** 81–95.

Langland, R. H., 2005a: Observation impact during the North Atlantic TreC-2003. *Mon. Wea. Rev.,* **133,** 2297–2309.

——, 2005b: Issues in targeted observing. *Quart. J. Roy. Meteor. Soc.,* **131,** 3409–3425.

——, and N. L. Baker, 2004: Estimation of observation impact using the NRL variational data assimilation adjoint system. *Tellus,* **56A,** 189–201.

——, and Coauthors, 1999: The North Pacific Experiment (NORPEX-98): Targeted observations for improved North American weather forecasts. *Bull. Amer. Meteor. Soc.,* **80,** 1363–1384.

——, M. A. Shapiro, and R. Gelaro, 2002: Initial condition sensitivity and error growth in forecasts of the 25 January 2000 East Coast snowstorm. *Mon. Wea. Rev.,* **130,** 957–974.

Laroche, S., M. Tanguay, A. Zadra, and J. Morneau, 2002: Use of adjoint sensitivity analysis to diagnose the CMC Global analysis performance: A case study. *Atmos.–Ocean,* **40** (4), 423–443.

Leutbecher, M., 2003: A reduced rank estimate of forecast error variance changes due to intermittent modifications of the observing network. *J. Atmos. Sci.,* **60,** 729–742.

Liu, Z. Q., and F. Rabier, 2002: The interaction between model resolution, observation resolution and observation density in data assimilation: A one-dimensional study. *Quart. J. Roy. Meteor. Soc.,* **128,** 1367–1386.

Mahidjiba, A., M. Buehner, and A. Zadra, 2007: Excitation of Rossby-wave trains: Optimal growth of forecast errors. *Meteor. Z.,* **16,** 665–673.

Molteni, F., R. Buizza, T. N. Palmer, and T. Petroliagis, 1996: The ECMWF ensemble prediction system: Methodology and validation. *Quart. J. Roy. Meteor. Soc.,* **122,** 73–120.

Petersen, G. N., and A. J. Thorpe, 2007: The impact on weather forecasts of targeted observations during A-TreC. *Quart. J. Roy. Meteor. Soc.,* **133,** 417–431.